Multichannel-quantum-defect-theory treatment of reactive collisions between electrons and BeH^{+}

S. Niyonzima, F. Lique, K. Chakrabarti, Å. Larson, A. E. Orel, and I. F. Schneider

Phys. Rev. A **87**, 022713 — Published 27 February 2013

DOI: 10.1103/PhysRevA.87.022713

Multichannel quantum defect theory treatment of reactive collisions between electrons and BeH^+

S. Niyonzima[1,2], F. Lique[1], K. Chakrabarti[3], Å. Larson[4], A. E. Orel[5] and I. F. Schneider[1*]
[1] *LOMC-UMR 6294 CNRS-Université du Havre, 25 Rue Philippe Lebon, BP 540-76 058 Le Havre Cedex, France*
[2] *Département de Physique, Fac. des Sciences, Université du Burundi, B.P. 2700 Bujumbura, Burundi*
[3] *Dept. of Mathematics, Scottish Church College, 1 & 3 Urquhart Sq., Kolkata 700 006, India*
[4] *Department of Physics, Stockholm University, AlbaNova University Center, S-106 91 Stockholm, Sweden*
[5] *Department of Chemical Engineering and Materials Science, University of California, Davis, California 95616, USA*
(Dated: February 5, 2013)

A theoretical treatment of dissociative recombination (DR), vibrational excitation (VE) and vibrational deexcitation (VdE) of the BeH^+ ion in its four lowest vibrational states ($X^1\Sigma^+, v_i^+ = 0, 1, 2, 3$) is reported. The multichannel quantum defect theory is used to determine cross sections and rate coefficients. Three electronic symmetries of BeH - $^2\Pi$, $^2\Sigma^+$, and $^2\Delta$ - have been included in the calculations. At low energies the DR is dominated by capture into states of $^2\Pi$ symmetry. Satisfactory agreement with results obtained using the wave packet approach is reached at intermediate energies despite significant differences at low energies. Cross sections and rate coefficients suitable for the modeling of the kinetics of BeH^+ in fusion plasmas and in the stellar atmospheres are presented and discussed.

I. INTRODUCTION

Beryllium has been proposed as a plasma facing material candidate in the edge of the International Thermonuclear Experimental Reactor (ITER) [1] in order to suppress chemical erosion of carbon in the main chamber [2]. The choice of beryllium is justified by its small impact on the plasma performance [3] since it should have a low tritium retention [4, 5]. The beryllium wall will be exposed to plasma heat and particles bombardment at the edge of the reactor and then it will undergo chemical erosion [4, 6, 7]. Consequently, the beryllium atoms will enter into the plasma, form molecular species like BeH, BeD and BeT due to reactions with atoms of the fuel (H, D, T) in the fusion device [4, 7] and will interact with other impurities. These molecules will be ionized by collisions with plasma electrons and move rapidly under the action of variable magnetic field. Ions and neutrals move towards the divertor. In the plasma described above, numerous atomic and molecular processes occur. Even though hydrogen isotopes, used as fuel in the fusion devices, dominate the evolution of the core plasma, in the low temperature edge/divertor regions (below 20000 K), the collisions between electrons and BeH^+ ions play a major role [8]. Therefore, studies (experimental or theoretical) of the above process are needed for plasmas diagnostics and modeling [9–11]. The BeH^+ ion can be destroyed by Dissociative Recombination (DR) [12]:

$$BeH^+ + e^- \longrightarrow Be + H \tag{1}$$

assisted by Vibrational Transitions (VT) - excitation (VE) and deexcitation (VdE):

$$BeH^+(v_i^+) + e^- \longrightarrow BeH^+(v_f^+) + e^- \tag{2}$$

and by Dissociative Excitation (DE) :

$$BeH^+ + e^- \longrightarrow Be^+ + H + e^-. \tag{3}$$

Here v_i^+ and v_f^+ are the initial and final vibrational quantum number of the ion respectively.

On the other hand, BeH and its associated ion BeH^+ have been identified in stars - including the sun (in sunspots) [13] - and comets [14, 15]. The accurate determination of physical and chemical conditions of these media also requires the knowledge of the relevant elementary processes involving these molecules among which the DR and VT of BeH^+ play a central role. Unfortunately, due to the high toxicity of beryllium, no measurement on electron scattering process with BeH^+ is available. Thus, calculations seem to be the only way to obtain these data. Theoretical studies proceed in two steps:
(i) solving the electronic part of the problem to determine relevant potential energy curves (PEC), couplings and autoionization widths and then
(ii) solving the nuclear part of the problem to compute cross sections and rate coefficients.

Quantum chemistry calculations on BeH/BeH^+ have been reported in Refs. [16–18]. In [16], adiabatic potential energy curves of the six lowest electronic states of $^1\Pi$, $^1\Sigma^+$,$^3\Pi$ and $^3\Sigma^+$ symmetries of BeH^+ have been computed using the multireference configuration interaction (MRCI) method. Full configuration interaction calculations by Pitarch-Ruiz at al. [18] provided adiabatic potential energy curves of the lower states of BeH. These calculations were preceded by the work of Machado et al. [17], which revealed the existence of a double minimum of the low lying excited $^2\Pi$ Rydberg states of the BeH molecule. Recently, by combining the MRCI method with electron scattering calculations using the complex-Kohn variational method [19] two of the present authors [12] calculated both adiabatic and quasidiabatic potential energy curves of excited states of BeH, hence providing data for the study of DR and VT of BeH^+.

* Corresponding author:ioan.schneider@univ-lehavre.fr

In the same article, the first theoretical predictions of the DR cross sections of BeH^+ in its two lowest vibrational states have been reported using the wave packet method [20]. Couplings between dissociative states and excited Rydberg states of BeH of $^2\Pi$, $^2\Sigma^+$ and $^2\Delta$ symmetries have been considered, leading to sharp oscillations of the cross sections. However, the wave packet (WP) technique may not be the most suitable approach at low collisional energies because the indirect mechanism through electronic capture into bound Rydberg states is only partially included. Indeed, only a limited number of such states were considered, and the vibronic couplings were neglected.

In this paper, we use the molecular structure data previously computed [12] in order to revisit the low/moderate energy electron impact collisions by a method based on the Multichannel Quantum Defect Theory (MQDT)[21, 22]. This allows a detailed approach of the indirect mechanism at very low energy and of the vibronic couplings between the ionization channels. We take the opportunity to enlarge the previous work [12] by studying the vibrational dependence of the DR cross section for initial vibrational quantum numbers $v_i^+ = 0, 1, 2, 3$. Furthermore, we address inelastic vibrational transitions in electron collisions, which are major competitors of the recombination process. The paper is organized as follows: Sec. II provides a brief description of the theoretical approach. Sec. III presents the computational details of this work and in Sec. IV, we present the DR and VT cross sections and rate coefficients of BeH^+ at low and intermediate energies/temperatures.

II. THEORETICAL APPROACH

The collision processes studied here involve two mechanisms:
(a) the *direct* process in which the electron is captured into a doubly excited dissociative state BeH^{**} of the neutral system leading either to two neutral atomic fragments Be and H or to autoionization:

$$BeH^+(v_i^+) + e^- \longrightarrow BeH^{**} \longrightarrow \begin{cases} Be + H \\ BeH^+(v_f^+) + e^- \end{cases} \quad (4)$$

(b) the *indirect* process consisting in the temporary capture of the electron into a singly excited bound Rydberg state BeH^*, predissociated by BeH^{**}:

$$\begin{aligned} BeH^+(v_i^+) + e^- &\longrightarrow BeH^* \longrightarrow BeH^{**} \\ BeH^{**} &\longrightarrow \begin{cases} Be + H \\ BeH^+(v_f^+) + e^- \end{cases} \end{aligned} \quad (5)$$

These processes are reactive collisions involving two different types of channels, namely dissociation channels (describing the atom-atom scattering) and ionization channels (describing electron-molecular ion scattering).

A channel is **open** if the total energy of the molecular system is higher than the energy of its fragmentation threshold, and **closed** in the opposite case. An ionization closed channel introduces in the calculation a series of Rydberg states differing only by the principal quantum number of the external electron [11]. Hence, the inclusion of the closed channels allows for the *indirect* mechanism, which interferes with the direct one resulting in the *total* process.

The dissociation and the ionization channels are coupled by the short range Rydberg-valence interaction accounted for at the electronic level first, through the R-dependent electronic coupling $V(R)$. According to [21], for a given dissociative state d_j, this coupling is given by:

$$V(R) = < \Phi_{d_j} | H_{el} | \Phi^{(el/ion)} >, \quad (6)$$

the integration being performed on the electronic coordinates of the total neutral system. Here H_{el} is the electronic part of the hamiltonian, Φ_{d_j} the electronic wavefunction of the neutral molecule dissociative state, and $\Phi^{(el/ion)}$ the electronic wavefunction describing the electron-ion scattering. As stated in [21], $V(R)$ is assumed to be independent on the energy of the outer electron, and an appropriate choice of the wavefunctions may result in real values for this quantity. However, the computation of this coupling by quantum chemistry methods is a very difficult task. Instead, one usually extracts its absolute value from the autoionization width $\Gamma(R)$, obtained from electron-ion scattering calculations [12, 23], using $V(R) = [\Gamma(R)/(2\pi)]^{1/2}$. The integration of this interaction on the internuclear motion leads to the construction of the interaction matrix $\mathcal{V}$:

$$\mathcal{V}_{d_j,v^+}(E) = \langle \chi_{d_j}(E) | V(R) | \chi_{v^+} \rangle, \quad (7)$$

where χ_{d_j} and χ_{v^+} represent the nuclear wave functions of the dissociative state d_j and of the vibrational state associated to an ionization channel respectively, and E is the total energy of the molecular system. This interaction is effective in the *reaction zone* only, characterized by small electron-ion and internuclear distances. Once the interaction matrix $\mathcal{V}$ is built, we determine the short range reaction matrix $\mathcal{K}$ by solving the Lippmann-Schwinger matrix equation:

$$\mathcal{K} = \mathcal{V} + \mathcal{V} \frac{1}{E - H_0} \mathcal{K}, \quad (8)$$

where H_0 is a zero-order Hamiltonian matrix of the molecular system under study. The solution adopted for the Lippmann-Schwinger equation depends on the strength of the interaction matrix elements [Equation (7)] and on its variations with the electron energy [24]. For weak couplings, this equation has a perturbative solution [25], which is exact at second order [24–26], provided that the electronic coupling $V(R)$ is energy-independent [24, 25]. In the energy representation, the elements of

the reaction matrix (8) write:

$$\mathcal{K}_{mn}(E^{'},E) = \mathcal{V}_{mn}(E^{'},E) + \sum_{q} \mathcal{P} \int dE^{''} \frac{\mathcal{V}_{mq}(E^{'},E^{''})}{E-E^{''}} \mathcal{K}_{qn}(E^{''},E) \quad (9)$$

m, n and q indicating dissociation (d_j type) or ionization (v^+ type) channels. It should be noted that within the quasidiabatic representation we are using, the interaction matrix $\mathcal{V}$ does not have nonvanishing matrix elements between two ionization channels (Rydberg-Rydberg interaction) or two dissociation channels (valence-valence interaction). As for the Rydberg-valence interaction matrix elements, which couple ionization to dissociation channels, they depend on the total energies E, $E^{'}$, $E^{"}$ involved in Eq. (9) through the relative kinetic energy release of the dissociation products [24].

In order to cast the result of the short range interaction in terms of phase shift, we diagonalize the $\mathcal{K}$ matrix:

$$\mathcal{K}U = -\frac{1}{\pi}\tan(\eta)U. \quad (10)$$

In the external region, the Born-Oppenheimer representation is no longer valid for the neutral molecule, and a frame transformation [22] is performed into a close-coupling representation, via the projection coefficients:

$$\mathcal{C}_{lv^+,\Lambda\alpha} = \sum_{v} U^{\Lambda}_{lv,\alpha} \langle \chi_{v^+}(R)| \cos(\pi\mu^{\Lambda}_{l}(R) + \eta^{\Lambda}_{\alpha})|\chi_{v}(R)\rangle \quad (11)$$

$$\mathcal{C}_{d,\Lambda\alpha} = U^{\Lambda}_{d\alpha} \cos\eta^{\Lambda}_{\alpha} \quad (12)$$

$$\mathcal{S}_{lv^+,\Lambda\alpha} = \sum_{v} U^{\Lambda}_{lv,\alpha} \langle \chi_{v^+}(R)| \sin(\pi\mu^{\Lambda}_{l}(R) + \eta^{\Lambda}_{\alpha})|\chi_{v}(R)\rangle \quad (13)$$

$$\mathcal{S}_{d,\Lambda\alpha} = U^{\Lambda}_{d\alpha} \sin\eta^{\Lambda}_{\alpha}. \quad (14)$$

Here the labels l, Λ, and α designate respectively the orbital quantum number (corresponding to a partial wave) of the outer electron, the quantum number associated to the projection of the total electronic angular momentum on the internuclear axis, and the eigenchannel defined through the diagonalization of the $\mathcal{K}$ reaction matrix. These coefficients result from the joint action of the two types of coupling driving the molecular dynamics in the curently described processes, i.e., the electronic coupling expressed by the eigenphases η and eigenvectors U of the reaction matrix, and the vibronic coupling between ionization channels expressed by the matrix elements involving the quantum defects $\mu^{\Lambda}_{l}(R)$. Starting from the matrices built on the elements defined in equations (11)-(14), the generalized scattering matrix is obtained and organized in an appropriate block-diagonal structure, accounting for open(o) and closed(c) channels:

$$X = \frac{\mathcal{C}+i\mathcal{S}}{\mathcal{C}-i\mathcal{S}} \qquad X = \begin{pmatrix} X_{oo} & X_{oc} \\ X_{co} & X_{cc} \end{pmatrix}. \quad (15)$$

Finally, the elimination of the closed ionization channels in the X matrix leads to the physical scattering matrix [27]:

$$S = X_{oo} - X_{oc}\frac{1}{X_{cc} - \exp(-i2\pi\nu)}X_{co} \quad (16)$$

and to the DR and VT cross sections for each neutral electronic symmetry (singlet/triplet g/u) and angular momentum quantum number Λ

$$\sigma^{sym,\Lambda}_{diss\leftarrow v^+_i} = \frac{\pi}{4\varepsilon}\rho^{sym,\Lambda}\sum_{l,j}|S_{d_j,lv^+_i}|^2; \quad (17)$$

$$\sigma^{sym,\Lambda}_{v^+_f\leftarrow v^+_i} = \frac{\pi}{4\varepsilon}\rho^{sym,\Lambda}\sum_{l,l'}|S_{l'v^+_f,lv^+_i} - \delta_{l'l}\delta_{v^+_f v^+_i}|^2; \quad (18)$$

and then the global cross sections:

$$\sigma_{diss\leftarrow v^+_i} = \sum_{\Lambda,sym}\sigma^{sym,\Lambda}_{diss\leftarrow v^+_i}, \quad (19)$$

$$\sigma_{v^+_f\leftarrow v^+_i} = \sum_{\Lambda,sym}\sigma^{sym,\Lambda}_{v^+_f\leftarrow v^+_i} \quad (20)$$

are generated. Here ε is the incident electron energy, $\rho^{sym,\Lambda}$ is the ratio between the multiplicities of the neutral system and of the ion, and $\exp(-2\pi\nu)$ labels a diagonal matrix whose nonvanishing elements $\exp(-2\pi\nu_{v^+})$ are built using the effective quantum numbers ν_{v^+} associated to the closed ionization v^+ channels.

The molecular data needed to perform the MQDT calculations have been produced by some of us and our coworkers (Roos *et al.* [12]) using *ab initio* Multireference Configuration Interaction (MRCI) calculations combined with electron scattering calculations. Adiabatic potential energy curves (PEC) have been calculated for the ground state of BeH^+ and for the excited states of BeH for each relevant symmetry. Using the complex Kohn variational method [19] electron scattering calculations were performed to determine energy positions and autoionization widths of the resonant states. A diabatization procedure [12] of BeH PEC followed in order to produce the data needed for the DR and VT study: the energies and autoionization widths of the dissociative states BeH^{**}, and the Rydberg states of temporary capture BeH^{*}. We show in Fig. 1 the quasidiabatic dissociative PEC and their electronic couplings with the ionization continuum of BeH in the $^2\Pi$, $^2\Sigma^+$, and $^2\Delta$ electronic symmetries.

III. COMPUTATIONAL DETAILS

Using the set of molecular data described above, we have performed a series of MQDT calculations of DR and VT cross sections, taking into account the direct and indirect processes. We have considered the target molecular ion on its lowest four vibrational levels (v^+_i =

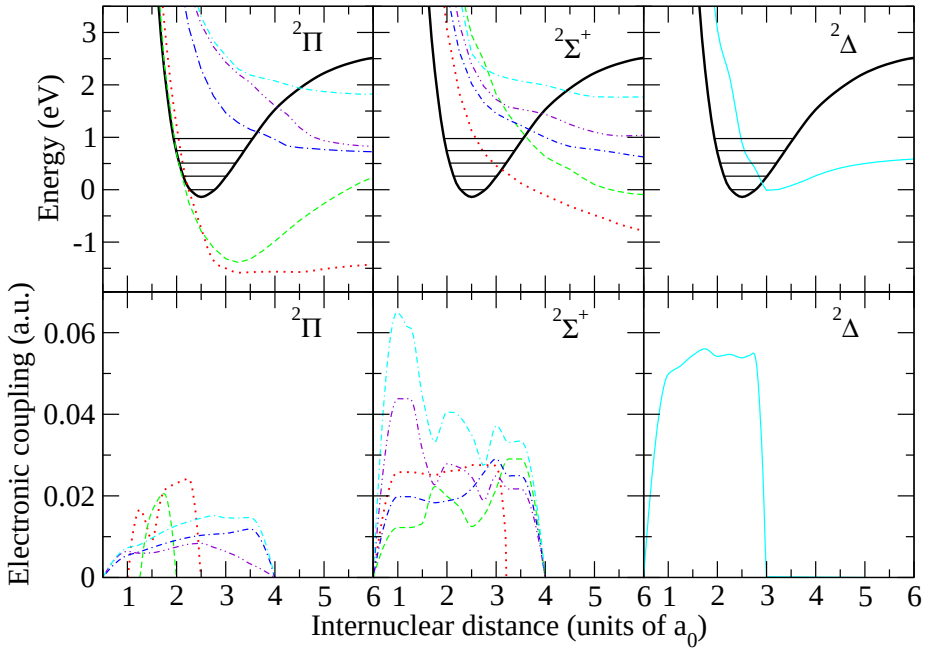

FIG. 1. *(Color online) Upper row: Potential energy curves of BeH$^+$ (thick black line) and dissociative states of BeH of $^2\Pi$, $^2\Sigma^+$, and $^2\Delta$ symmetries. Lower row: Electronic couplings between the dissociative states of BeH and the ionization continuum.*

$0-3$) of its ground electronic state. The cross sections are calculated separately for each symmetry (involving all the relevant dissociative states within the symmetry) and are summed to give the global cross section.

We have explored the energy range 10^{-3} - 2.7 eV of the incident electron, which corresponds to a total energy of the system below the dissociation limit of its ground electronic state. The energy step is 0.01 meV. All dissociative states plotted in Fig. 1 and all the 18 discrete vibrational states of the ion have been included in the calculations. From the quasidiabatic PEC's of the Rydberg states of Ref.[12], we have extracted quantum defects defining the Rydberg series of the $^2\Pi$ and $^2\Sigma^+$ symmetries of BeH. Unfortunately, for the $^2\Delta$ symmetry, only one dissociative state was available from the data of Ref.[12] and we have taken into account only the direct process for this symmetry. Taking into account the fact that the dissociative states belong to Rydberg series of states converging to the excited ion core, autoionization widths of the very highly excited states of these series have also been calculated, using the Rydberg scaling law. They have been added to that of the most excited resonant state available for both $^2\Pi$ and $^2\Sigma^+$ symmetry of BeH. Consequently, for each of these symmetries, this state becomes an effective one, and accounts for the contribution of the higher excited states of the Rydberg series[28]. The integration appearing in equation (7) has been performed on a grid of internuclear distance of 2450 points ranging from 0.5 to 30.5 units of a_0 (a_0=0.0529177 nm).

In order to obtain the thermal rate coefficients, we have convoluted the DR and VT cross sections with the Maxwellian isotropic distribution function for velocities of the free electrons [29] :

$$\alpha(T) = \frac{8\pi}{(2\pi kT)^{3/2}} \int_0^{+\infty} \sigma(\varepsilon)\varepsilon \exp(-\varepsilon/kT)d\varepsilon, \quad (21)$$

where σ is the cross sections given by (19) or (20) and k is the Boltzmann constant.

IV. RESULTS AND DISCUSSIONS

In this section, we present the results for DR and VT cross sections and rate coefficients of BeH$^+$ in its four lowest vibrational levels ($v_i^+ = 0, 1, 2, 3$) of the electronic ground state ($X^1\Sigma^+$).

A. Cross sections

1. *Dissociative recombination*

In Fig. 2 we show the contributions of the relevant symmetries to the *direct* DR cross section of BeH$^+$ in its ground vibrational state, as well as the total direct cross section obtained after summation.

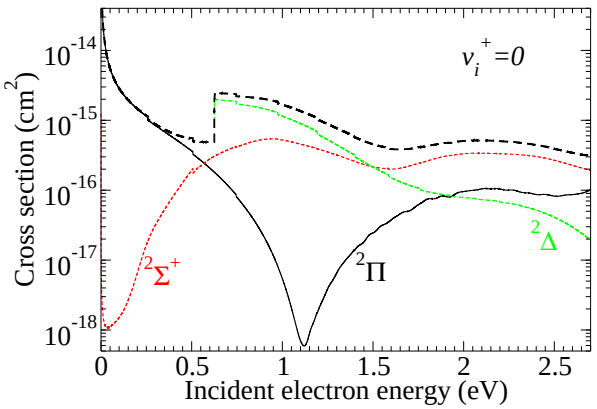

FIG. 2. *(Color online) Contribution of relevant symmetries to the direct DR cross section of BeH^+ in its ground vibrational state. The thick dashed line represents the cross section summed over all electronic symmetries.*

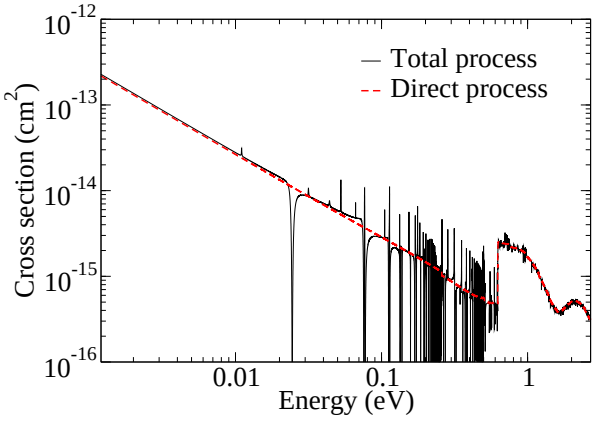

FIG. 3. *(Color online) Direct (dashed red online thick line) and total (oscillating black thin line) DR cross sections of BeH^+ in its ground state.*

First of all, the $^2\Delta$ symmetry does not allow DR for collisional energies below 0.6 eV. This energy corresponds to the energy threshold opening of its lowest dissociative channel. The $^2\Pi$ symmetry dominates the process at low energies because the PEC of the corresponding first and second dissociative states cross the ion PEC in the vicinity of its ground vibrational level (see Fig. 1). Its importance decreases strongly with energy until around 1 eV, when a strong revival occurs due to the opening of the next two highly excited dissociative states. At intermediate energies, the $^2\Sigma^+$, and $^2\Delta$ electronic symmetries contribute significantly to the DR process due to the relatively strong electronic couplings between dissociative states and the electron-ion continuum.

At low and intermediate collision energies below the ion dissociation limit, the colliding electron may transfer its kinetic energy to the vibrational motion of the BeH^+ ion and then, may be temporarily captured into a bound Rydberg state of the neutral, BeH^*, as described by equations [(11-14)]. This bound state is predissociated by dissociative states BeH^{**} due to the Rydberg-valence interaction [equation (7)], resulting in the total (direct and indirect) mechanism [equations (4) and (5)]. In Fig. 3, we present the direct and total DR cross section (summed over all symmetries). The total cross section is characterized by a rich resonant structure. Figure 3 shows that the indirect process is relatively weak with respect to the direct one in this case.

Figure 4 displays the dependence of the direct DR cross section on the initial vibrational level of the ion target for each electronic symmetry. The DR through $^2\Pi$ symmetry for $v_i^+ = 0$ and $v_i^+ = 1$ dominates the process down to zero electron energy because of the crossings between its two lowest dissociative states and the BeH^+ PEC close to the classical turning points of these vibrational states (Fig. 1). The DR mainly occurs through $^2\Pi$ and $^2\Sigma^+$ symmetries for $v_i^+ = 2$ and through $^2\Pi$ and $^2\Delta$ symmetries for $v_i^+ = 3$ due to similar favorable crossings and, respectively, on the relative strong electronic coupling between the dissociative state of the $^2\Delta$ symmetry and the ionization continuum. We note stair steps for $v_i^+ = 0$ and $v_i^+ = 1$ corresponding to the opening of the dissociative channel of $^2\Delta$ symmetry. This does not appear for $v_i^+ = 3$ because this channel is open even at zero electron energy. These cross sections are summed over all symmetries and displayed in Fig. 5.

2. *Vibrational excitation*

The electron impact on the molecular cation may also lead to vibrational excitation (VE), which competes with the DR reaction. These two processes are intimately related and modelled simultaneously, as described by equations (17) and (18). Figure 6 displays the VE cross section of $BeH^+(v_i^+ = 0)$ obtained by a summation over all final vibrational states, v_f^+ of the ion. Both the direct and total (direct and indirect) processes are considered. Similar to what was found in the total DR cross section (Fig. 3), sharp oscillations appear in the total cross section of VE. Despite these sharp oscillations, we note that the direct and total DR and VE cross section have the same order of magnitude for all the energy range explored in this work and hence DR and VE are competitive processes at intermediate electron energies. The stair steps near 0.27 and 0.5 eV correspond to the opening of ionization channels. The huge rise near 0.6 eV corresponds to the opening of the dissociation channel of $^2\Delta$ and confirms the strongly resonant character of these vibrational transitions [23]. Indeed, the BeH^+/BeH system is subject to Rydberg-valence interactions, quantitatively expressed through the elements of the interaction matrix $\mathcal{V}_{d_j,v^+}(E)$. Consequently, the major pathway of a vibrational transition $v_i^+ \to v_f^+$ is of the type $v_i^+ \to d_j \to v_f^+$, the dissociative channels d_j being the doorways to the interchannel interactions.

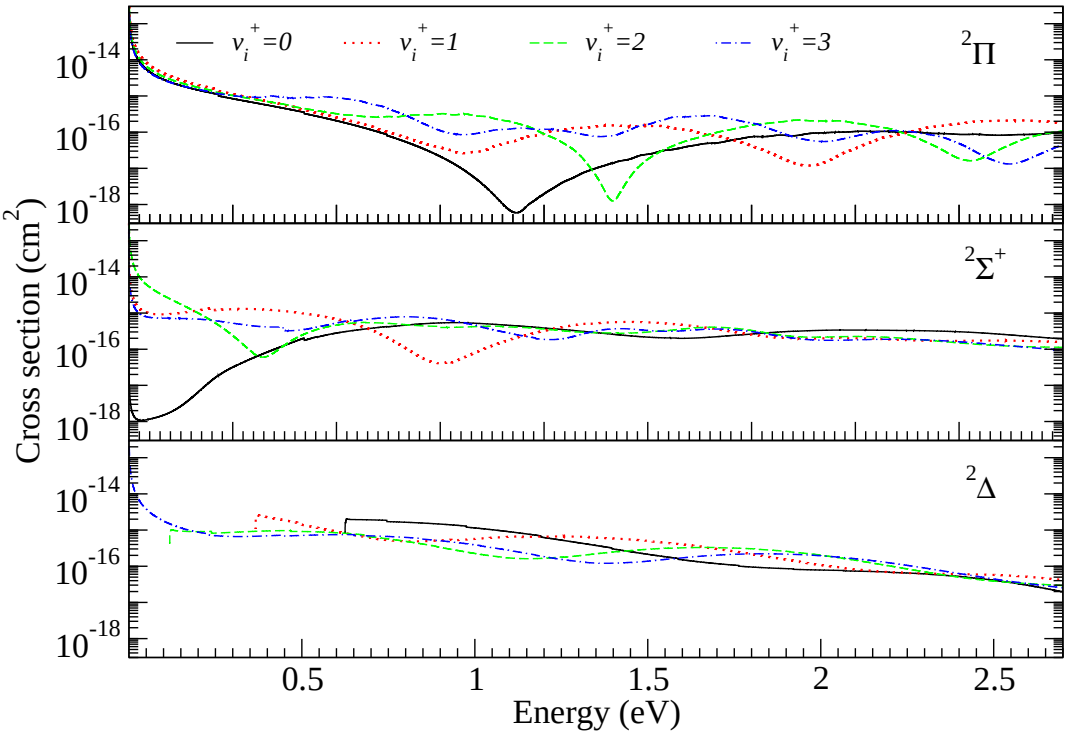

FIG. 4. *(Color online) Vibrational dependence of the direct DR cross section of BeH^+ for each electronic symmetry (v_i^+ indicates the initial vibrational quantum number of the target ion).*

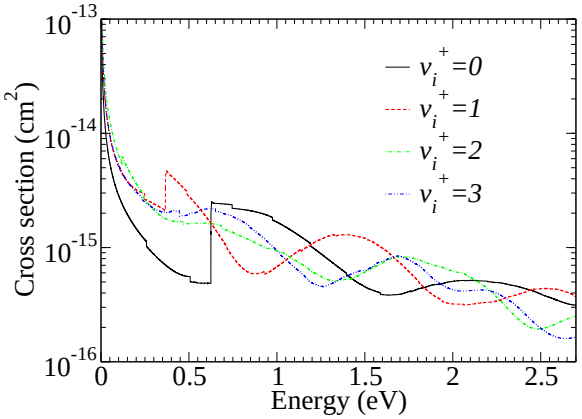

FIG. 5. *(Color online) Vibrational dependence of the direct DR cross section of BeH^+ (v_i^+ stands for the vibrational quantum number of the target ion).*

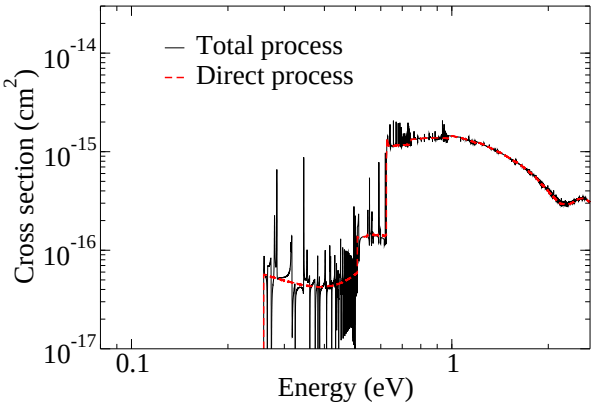

FIG. 6. *(Color online) Direct (red thick line) and total (oscillating black thin line) VE cross sections of BeH^+ in its ground state. The cross sections are summed over all final vibrational levels BeH^+ states.*

3. Comparison MQDT/WP

As mentioned in the introduction, a previous theoretical study of DR of BeH^+ used the wave packet (WP) technique [12]. In Figs. 7 and 8, we show a comparison between the direct and total DR cross sections, respectively computed by MQDT and WP methods. According to Fig. 7 it is obvious that the two methods produce sim-

ilar results for the direct mechanism. However, slight

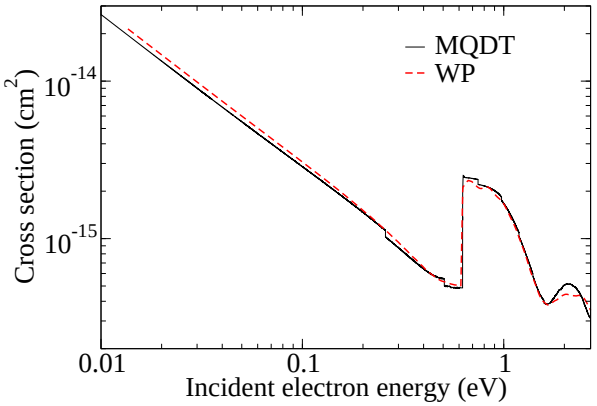

FIG. 7. *(Color online) Comparison between MQDT (solid black) and WP methods (dashed red online) direct DR cross sections of BeH^+ in its vibrational ground state.*

deviations between MQDT and WP results are found at low collision energies that could be explained by the fact that the WP method is based on a local approximation for including autoionization. Figure 8 highlights the discrepancy between the total DR cross sections by MQDT and WP methods. The previously used WP approach included electronic couplings to Rydberg states. However, for an accurate description of the indirect mechanism, a high number of Rydberg states have to be included as well as the electronic and nonadiabatic couplings [30]. MQDT fully manages the infinity of possible resonant captures, as well as the nonadiabatic interchannel couplings, and therefore is more appropriate to produce accurate cross sections at low energy, when most of the ionization channels are closed [31].

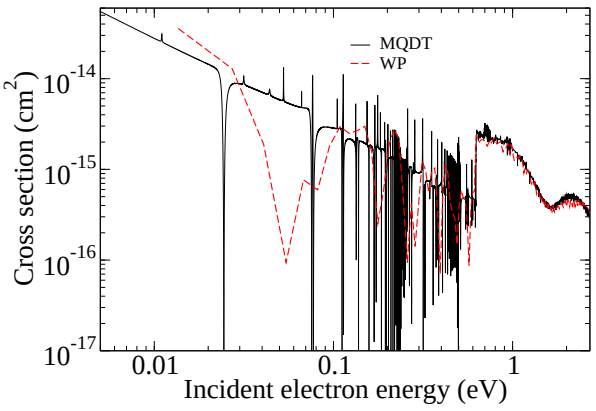

FIG. 8. *(Color online) Comparison between MQDT (solid black line) and wave packet (dashed red line) total DR cross sections of BeH^+ ($v_i^+ = 0$).*

B. Rate coefficients

We used the calculated DR and VE cross sections to obtain, by Maxwell averaging, the DR and VE thermal rate coefficients up to 5000 K. Figure 9 displays the comparison between direct and total DR rate coefficients corresponding to the cross sections of Fig. 3. The resonances do not significantly affect the magnitude of DR rate coefficients in the case of BeH^+ unlike what has been found for other systems like H_2^+ and HD^+ [31]. This feature comes from the weak electronic coupling of the closed channels to the dominant dissociative states, due to the unfavorable crossings of the potential energy curves illustrated in Fig. 1, as well as from their weak nonadiabatic coupling to the entrance ionization channel, due to the smooth variation of the quantum defects of the Rydberg states with the internuclear distance.

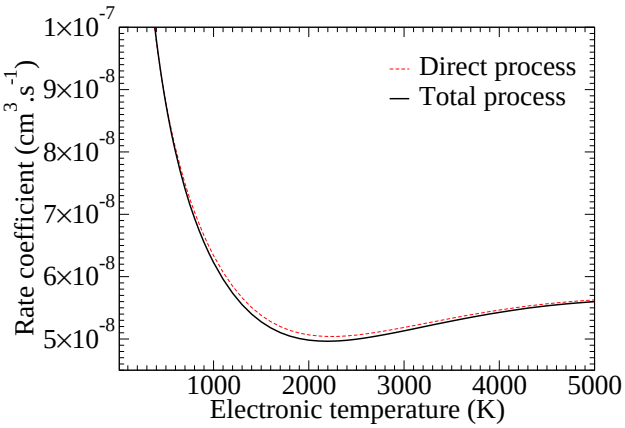

FIG. 9. *(Color online) Direct and total DR rate coefficients of BeH^+ in its ground vibrational state.*

In Fig. 10, we show the total DR and VE rate coefficients of BeH^+ in its ground vibrational state. The DR rate coefficients obtained by Roos *et al.* [12] are plotted too, for temperature higher than 500 K. In the same figure we display the global rate coefficients for the VE from the ground state ($v_i^+ = 0$ to *all* excited vibrational levels ($v_f^+ = 1, 2$,...etc.) for the total mechanism. Whereas this latter process is negligible with respect to the DR at low temperature, it becomes a serious competitor above 3000 K.

Figure 11 shows the total DR and VT rate coefficients for the three lowest excited vibrational levels of the ion, in comparison with that corresponding to the ground vibrational state. It illustrates a relatively fast DR of BeH^+ in its $v_i^+ = 2$ level, as well as a relatively fast VdE for $v_i^+ = 3$, at low temperature.

Figure 12 displays the rates of the state to state vibrational transitions. For all initial vibrational levels, curves of same color represent the total VE and VdE rate coefficients related to the same $\Delta v = v_f^+ - v_i^+$. For all of the initial vibrational levels considered, the evolution of the excitation rate coefficient with Δv and with the

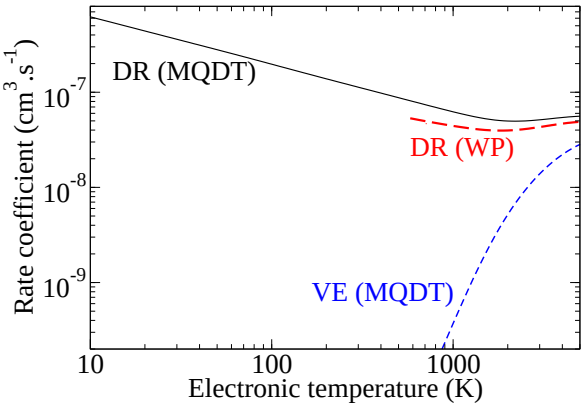

FIG. 10. *(Color online) Comparison between MQDT (present calculations) and WP (Ross et al.[12]) total DR rate coefficients of BeH^+ in its ground state. The MQDT-computed rate coefficient for total VE of BeH^+ from its ground vibrational state into all the vibrational excited states is also presented.*

temperature is quite similar.

V. CONCLUSIONS

The present paper extends the initial study [12] of the BeH^+ reactive collisions with electrons on several aspects.

The first is the detailed analysis of the dissociative recombination at very low (close to zero) energy of the incident electron. This required the use of an MQDT-based approach, able to fully account for the temporary captures into Rydberg bound states, as well as for the vibronic coupling between the relevant ionization channels. The MQDT-calculations resulted in accurate cross sections in the case of very slow electrons - a case of major interest for cold astrophysical media - and agree well at higher energy with those performed by the wave packet method.

The second aspect is the evaluation of the vibrational transitions. We produced cross sections and rate coefficients for vibrational excitation and deexcitation, never computed before, and certainly useful for the detailed kinetics modeling [26, 32], either in astrophysics, or in the cold plasma close to the wall of the fusion devices.

The third is the extension to higher vibrational states of BeH^+: our data concern the lowest four vibrational levels of the target, and all the vibrational levels of the ion as final states of the vibrational transitions.

Our approach of the vibrational excitation opens the way to the study of the dissociative excitation [33], occuring above the dissociative threshold of the molecular ion. This process, very important in the modeling of the plasma/wall interaction [4], is the object of an ongoing study, devoted to the reactive collisions at high (above 3 eV) energy range of the incident electron.

ACKNOWLEDGMENTS

S. Niyonzima acknowledges the Burundi Government for the Ph.D grant. We acknowledge the scientific and financial support from the European Space Agency (ESTEC 21790/08/NL/HE) and the International Atomic Energy Agency, (CRP "Light Element atom, Molecule and Radical Behaviour in the Divertor and Edge Plasma Regions"). We have been supported by the French network "Fédération de Recherche Fusion Magnétique Contrôlée" (CEA, EFDA, EURATOM), the ANR-contract "SUMOSTAI". Financial support from Région Haute Normandie has been provided to us through the CPER (CNRT/"Energie, Electronique, Matériaux") and "Institut d'Energie, Fluides et Environnement" (Rouen-Le Havre). AEO acknowledges support from the National Science Foundation under grant PHY-08-55092 and ÅL is supported by the Swedish research council (Vetenskapsrådet).

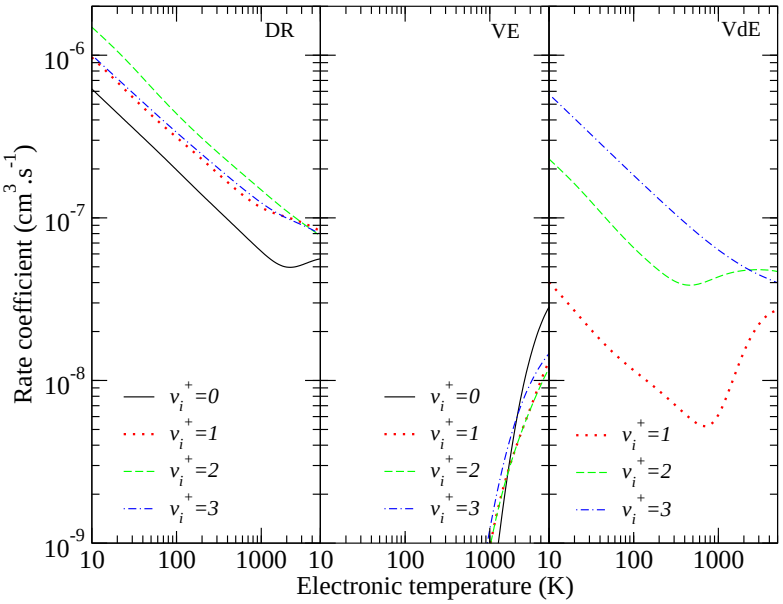

FIG. 11. *(Color online) Vibrational dependence of the total DR, VE and VdE rate coefficients of* BeH^+ *(*v_i^+ *stands for the vibrational quantum number of the target ion).*

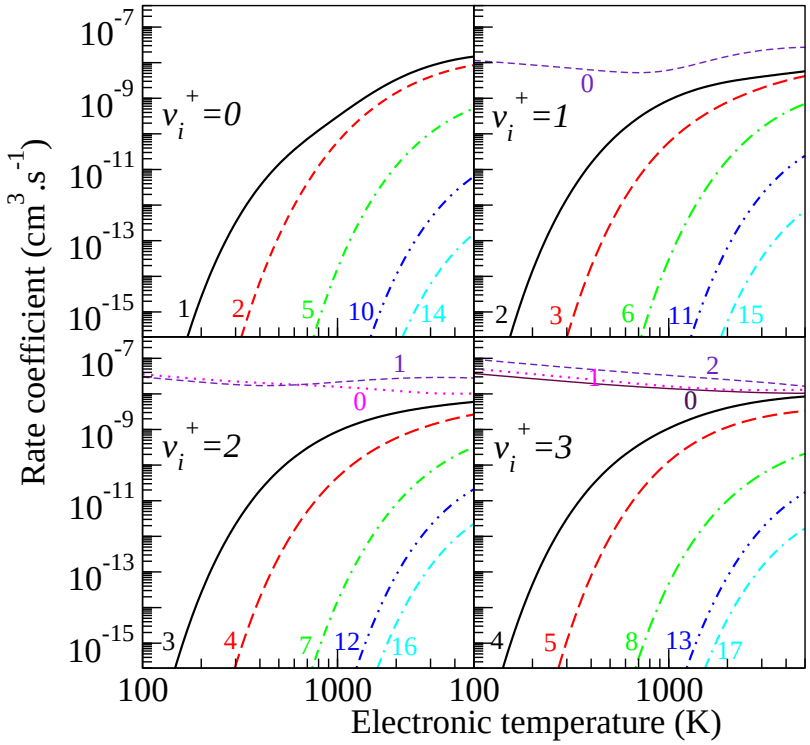

FIG. 12. *(Color online) State to state VE and VdE rate coefficients of BeH^+ initially on one of its four lowest vibrational levels, v_i^+. The final vibrational quantum number of BeH^+ is indicated on each curve.*

[1] http://www.iter.org/proj/iterandbeyond (2012).

[2] R. E. H. Clark and D. Reiter, *Nuclear Fusion Research: Understanding Plasma-Surface Interactions*, edited by Clark, R. E. H. and Reiter, D., Springer series in Chemical Physics, Vol. 78 (Springer Berlin Heidelberg, 2005).

[3] M. Shimada, D. Campbell, V. Mukhovatov, M. Fujiwara, N. Kirneva, K. Lackner, M. Nagami, V. Pustovitov, N. Uckan, J. Wesley, N. Asakura, A. Costley, A. Donn, E. Doyle, A. Fasoli, C. Gormezano, Y. Gribov, O. Gruber, T. Hender, W. Houlberg, S. Ide, Y. Kamada, A. Leonard, B. Lipschultz, A. Loarte, K. Miyamoto, V. Mukhovatov, T. Osborne, A. Polevoi, and A. Sips, Nucl. Fusion **47**, S1 (2007).

[4] R. Celiberto, R. K. Janev, and D. Reiter, Plasma Phys. Control. Fusion **54**, 035012 (2012).

[5] J. N. Brooks, D. N. Ruzic, and D. B. Hayden, Fusion Engineering and Design **37**, 455 (1997).

[6] V. Philipps, Phys. Scr. **123**, 24 (2006).

[7] C. Björkas, K. Vörtler, K. Nordlund, D. Nishijima, and R. Doerner, New J. Phys. **11**, 123017 (2009).

[8] K. Sergei, Plasma Phys. Control. Fusion **53**, 074017 (2011).

[9] V. Kokoouline, C. H. Greene, and B. D. Esry, Nature **412**, 891 (2001).

[10] B. J. McCall, A. J. Huneycutt, R. J. Saykally, T. R. Geballe, N. Djuric, G. H. Dunn, J. Semaniak, O. Novotny, A. Al-Khalili, A. Ehlerding, F. Hellberg, S. Kalhori, A. Neau, R. Thomas, F. Österdahl, and M. Larsson, Nature **422**, 500 (2003).

[11] I. F. Schneider, O. Dulieu, A. Giusti-Suzor, and E. Roueff, Astrophys. J. **424**, 983 (1994).

[12] J. B. Roos, M. Larsson, Å. Larson, and A. E. Orel, Phys. Rev. A **80**, 012501 (2009).

[13] V. P. Gaur, M. C. Pande, and B. M. Tripathi, Bull. Astron. Inst. Czech. **24**, 138 (1973).

[14] A. J. Sauval and J. B. Tatum, Astrophys. J. Suppl. Ser. **56**, 193 (1984).

[15] R. Shanmugavel, S. P. Bagare, and N. Rajamanickam, Serb. Astron. J. **173**, 83 (2006).

[16] B. M. Francisco and R. O. Fernando, J. Chem. Phys. **94**, 7237 (1991).

[17] F. Machado, O. Robertoneto, and F. Ornellas, Chem. Phys. Lett. **284**, 293 (1998).

[18] J. Pitarch-Ruiz, J. Sánchez-Marin, A. M. Velasco, and I. Martin, J. Chem. Phys. **129**, 054310 (2008).

[19] T. N. Rescigno, C. W. McCurdy, A. E. Orel, and B. H. Lengsfield III, *The Complex Kohn Variational Method in Computational Methods for Electron-Molecule Scattering*, edited by W. H. Huo, & F.A. Gianturco (Plenum, New York, 1995).

[20] A. E. Orel, J. Phys.: Conf. Ser. **4**, 142 (2005).

[21] A. Giusti, J. Phys. B **13**, 3867 (1980).

[22] I. F. Schneider, I. Rabadán, L. Carata, L. H. Andersen, A. Suzor-Weiner, and J. Tennyson, J. Phys. B **33**, 4849 (2000).

[23] K. Nakashima, H. Takagi, and H. Nakamura, J. Chem. Phys. **86**, 726 (1987).

[24] V. Ngassam, A. Florescu, L. Pichl, I. F. Schneider, O. Motapon, and A. Suzor-Weiner, Eur. Phys. J. D **26**, 165 (2003).

[25] A. I. Florescu, V. Ngassam, I. F. Schneider, and A. Suzor-Weiner, J. Phys. B **36**, 1205 (2003).

[26] O. Motapon, M. Fifirig, A. Florescu, F. O. Waffeu Tamo, O. Crumeyrolle, G. Varin-Bréant, A. Bultel, P. Vervisch, J. Tennyson, and I. F. Schneider, Plasma Sources Sci. Technol. **15**, 23 (2006).

[27] M. J. Seaton, Rep. Prog. Phys. **46**, 167 (1983).

[28] C. Strömholm, I. F. Schneider, G. Sundström, L. Carata, H. Danared, S. Datz, O. Dulieu, A. Källberg, M. Af Ugglas, X. Urbain, V. Zengin, A. Suzor-Weiner, and M. Larsson, Phys. Rev. A **52**, 4320 (1995).

[29] K. C. Mathur, A. N. Tripathi, and S. K. Joshi, Astrophys. J. **165**, 425 (1971).

[30] S. Morisset, L. Pichl, A. E. Orel, and I. F. Schneider, Phys. Rev. A **76**, 042702 (2007).

[31] F. O. Waffeu Tamo, H. Buhr, O. Motapon, S. Altevogt, V. M. Andrianarijaona, M. Grieser, L. Lammich, M. Lestinsky, M. Motsch, I. Nevo, S. Novotny, D. A. Orlov, H. B. Pedersen, D. Schwalm, F. Sprenger, X. Urbain, U. Weigel, A. Wolf, and I. F. Schneider, Phys. Rev. A **84**, 022710 (2011).

[32] A. Bultel, B. G. Chéron, A. Bourdon, O. Motapon, and I. F. Schneider, Phys. of Plasmas **13**, 043502 (2006).

[33] K. Chakrabarti et al., submitted (2012).